Supplementary Information

Ionic Complex Engineered Topologically Reconfigurable Salt-Resistant Hydrogels with Simultaneously Enhanced Swelling and Mechanical Properties

Lingling Ren[1](任玲玲), Guoxuan Ma[1](马澴炫), Zheng Wang[1](王峥), Shuang Liu[1](刘爽), Haoran Cheng[2]*(程浩然), David A. Weitz[3], Liyuan Zhang[1]*(张丽媛)

1. School of Petroleum Engineering, China University of Petroleum (East China), Qingdao 266580, China;
2. College of Chemical Engineering, Qingdao University Science and Technology, Qingdao 266042, China;
3. School of Engineering and Applied Sciences, Harvard University, Cambridge, Massachusetts 02138, United States.

Address correspondence to: liyuanzhang@upc.edu.cn , chenghaoran@qust.edu.cn

Table S1. The detailed preparation formula of the single-network hydrogels.

NO.	AMPS(M)	KA(M)	PEGDA(M)	Description
1	0.01	0.0006	0.003	Too brittle, cannot proceed with subsequent experiments
2	0.01	0.0006	0.002	Too brittle, cannot proceed with subsequent experiments
3	0.01	0.0006	0.001	Too brittle, cannot proceed with subsequent experiments
4	0.01	0.0006	0.0007	Too brittle, cannot proceed with subsequent experiments
5	0.01	0.0006	0.0004	Can proceed with subsequent experiments

Table S2. The detailed formula of the second network.

AM(M)	SBVI(M)	KA(M)	PEGDA(M)
0.1	0.014	0.0006	0.00016
0.1	0.014	0.0006	0.00031
0.1	0.014	0.0006	0.00061
0.1	0.014	0.0006	0.0012
0.1	0.014	0.0006	0.0018
0.1	0.014	0.0006	0.0024
0.1	0.028	0.0006	0.00031
0.1	0.042	0.0006	0.00031
0.1	0.056	0.0006	0.00031
0.1	0.07	0.0006	0.00031

Table S3. Formula of the simulated formation brine.

Ionic types	Na^+	Ca^{2+}	Mg^{2+}	Cl^-	Total
Concentration ($\times 10^3$ mg/L)	58.07	12.02	4.86	125.00	200

Table S4. Comparison of reported functional zwitterionic hydrogels.

Topic	Novelty	Functional properties	Ref.
Ion-triggered reconfigurable hydrogels	Double network strategy: the first network is AMPS and the second network is AM-SBVI; network topological adaptation	Salt-enhanced mechanical and swelling properties	This paper
Salt-responsive hydrogels	Semi-interpenetrating double network: polycationic (polyMETAC/HEAA) layer with polyelectrolyte effect and polyzwitterionic (polyVBIPS) layer with antipolyelectrolyte effect	Enabling reversible bending actuation through differential dimensional change	[1]
Salt-responsive hydrogel	Double network strategy: loosely cross-linked zwitterionic pSBVI networks into the highly cross-linked cationic pTMAEMA	Effective antimicrobial properties and surface regeneration.	[2]

Topic	Novelty	Functional properties	Ref.
Water-electricity co-generation gel	Molecularly engineered: incorporated phenyl-methylene-imidazole motif greatly enhances the salt binding ability and strengthens anti-polyelectrolyte effect	Boosted hydration, high salt tolerance, ultra-low evaporation enthalpy, durable anti-microbial ability, optimized water transport channel	3
Tough, non-swelling zwitterionic Hydrogel	Double network strategy: PVA, PSBMA; hofmeister-effect-assisted crystallization	Ultra-high toughness , non-swelling, long-term stability (>1 month) in harsh aquatic conditions	4
Electrochemical hydrogel	Molecularly engineered zwitterionic microgels as functional cross-linking domains within a highly entangled PAM network	Toughness 1450.8 kJ m^{-3}, low hysteresis, fatigue-resistant, conductivity 52.9 mS cm^{-1}, stable capacitance retention	5
Tough nonfouling zwitterionic hydrogels in saline	Pure zwitterionic triple-network with electrostatic interactions and entanglements as energy dissipation mechanisms	Compressive fracture stress of 18.2MPa in saline conditions, toughness of1.62 MJ m^{-3}, Young's modulusof 0.66 ± 0.03 MPa	6
Euryhaline hydrogels	Integration of two polymer segments with complementary salinity tolerances，internal dynamic complementary crosslinks	Stable water retention, constant swelling properties, and low-adhesion to oil in aqueous environments over a wide range of salinity.	7
Microphase-separated elastic ionic hydrogel	Double network strategy: zwitterions in the first network with highly entangled polymer chains; ultrasoft polyelectrolyte as the second network	Pressure sensitivity ~0.4 kPa^{-1}; temperature coefficient~1.5%·$°C^{-1}$, maintains stable signals under large strains and temperature fluctuations	8
Sulfonic-based zwitterionic hydrogel electrolyte	Directly exploit the Anti-Polyelectrolyte Effect of zwitterions to regulate the electrochemical stability window	Wide electrochemical stability window, high ionic conductivity , high working voltage, capacity, and energy density	9
Hygroscopic salt-hydrogel	Salting-in effect possessed by a zwitterionic hydrogel provide a new way to design more advanced composite sorbents	Facilitate water vapor sorption; enhanced swelling behavior in salt solutions	10

acrylamide (AM), poly([2-(methacryloyloxy)ethyl]trimethylammonium chloride) (polyMETAC), poly(3-(1-(4-vinylbenzyl)-1H-benzo[d]imidazol-3-ium-3-yl)propane-1-sulfonate) (polyVBIPS), poly(sulfobetaine vinylimidazole) (pSBVI), poly((trimethylamino)ethyl methacrylate chloride) (pTMAEMA), polyvinyl alcohol (PVA), poly(sulfobetaine methacrylate) (PSBMA), diallyldimethyl-ammonium chloride (DADMAC), polyacrylamide (PAM) poly(N-isopropylacrylamide) (PNIPAM).

Table S5. The detailed data of Figure 3L of energy calculation results.

Samples \ Parameters	F_{mix} (J/m^3)	F_{el} (J/m^3)	F_{assoc} (J/m^3)	F_{ion} (J/m^3)	F_{total} (J/m^3)
water	-2.94×10^6	4.46×10^4	-6.17×10^3	0	-2.9×10^6
20g/LNaCl	-2.74×10^6	5.32×10^4	-6.66×10^3	1.045×10^3	-2.692×10^6
100g/LNaCl	-2.65×10^6	8.61×10^4	-1.07×10^4	2.02×10^2	-2.574×10^6
200g/LNaCl	-2.41×10^6	1.22×10^5	-1.40×10^4	0.854×10^2	-2.302×10^6
Formation brine	-2.73×10^6	5.93×10^4	-3.38×10^3	1.09×10^2	-2.674×10^6

Table S6. The fundamental formation parameters of cores.

Core	Length (cm)	Diameter (cm)	Porosity (%)
1	7.002	2.528	29.91

2	6.992	2.524	29.13

Table S7. Displacement test results.

Core state	Before injection	After injection	After degradation
Flow rate (mL/min)	1	0.5	1
Pressure drop (MPa)	0.02	2.51	0.06
Permeability (mD)	120.6	0.962	40.2

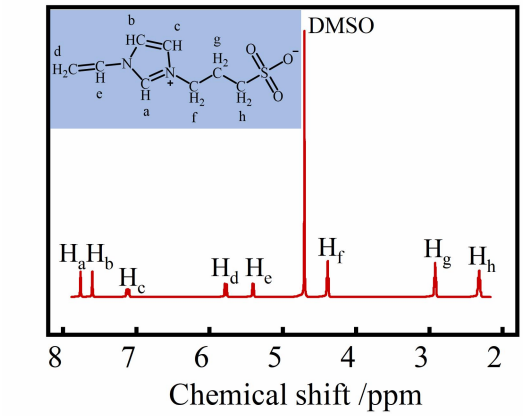

Figure S1. NMR characterization of SBVI. NMR measurement is performed using deuterated dimethyl sulfoxide as the solvent at 25 °C on a Bruker AVANCE III HD superconducting Fourier transform nuclear magnetic resonance spectrometer (400 MHz).

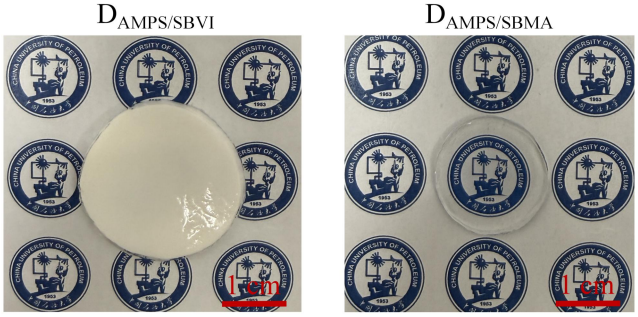

Figure S2. Morphological images of $D_{AMPS\text{-}SBVI}$ and $D_{AMPS/SBMA}$ hydrogels after swelling in water. $D_{AMPS/SBVI}$: The first network is AMPS and the second network is SBVI. $D_{AMPS/SBMA}$: The first network is AMPS and the second network is SBMA.

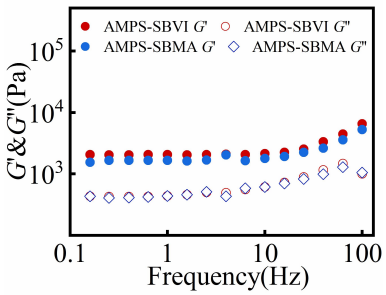

Figure S3. Rheological properties of $D_{AMPS\text{-}SBVI}$ and $D_{AMPS/SBMA}$ hydrogels after swelling in water. $D_{AMPS/SBVI}$: The first network is AMPS and the second network is SBVI. $D_{AMPS/SBMA}$: The first network is AMPS and the second network is SBMA.

The unusual plateau observed in the tensile stress-strain curve

We conduct systematic control experiments to explore the unusual plateau observed in the tensile stress-strain curve. First, to rule out the possibility of grip slipping during the tensile test, we mark the grip positions on the hydrogel sample before each test and examined the marks after the test, as shown in Figure S4. The results show that the marker positions remained unchanged before and after stretching, indicating that no slippage occurred throughout the entire testing process, and therefore the plateau cannot be attributed to grip slippage.

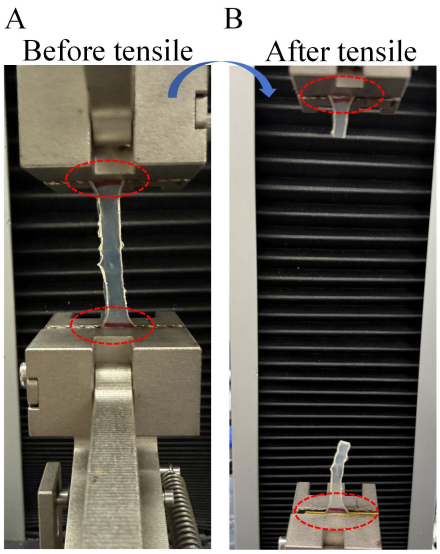

Figure S4. Schematic diagram of grip's position before (A) and after (B) hydrogel stretching.

We also found that the appearance of the plateau is strongly correlated with the content of the second network. As shown in Figure S5, a clear plateau is observed only in samples containing sufficiently high second network content, whereas no obvious plateau appears in samples with lower second-network content. This composition dependence indicates that the plateau is structurally associated with the architecture of the double-network hydrogel rather than arising from a random testing artifact.

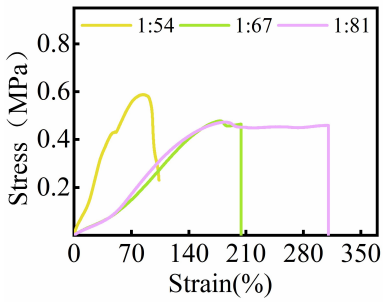

Figure S5. The tensile stress-strain curve of hydrogels. For the first network, the AMPS, initiator and crosslinker are 0.01 M, 0.0006 M, and 0.0004 M, respectively. For the second network, the AM, SBVI, the initiator and the crosslinker are 0.1 M, 0.014 M, 0.0006 M, and 0.00061 M, respectively. The feed molar ratio of first and second network is from 1:81 to 1:54.

Direct observation of the stretching process for samples exhibiting the plateau shows that the deformation can be divided into three stages, as illustrated in Figure S6 and Figure S7. In Stage I, the sample deforms approximately elastically, and the stress increases with strain. In Stage II, localized damage initiates, as evidenced by the appearance of a small crack and a slight stress softening. However, this damage does not lead to immediate catastrophic failure of the specimen. In Stage III, the hydrogel undergoes pronounced necking, and the necked region gradually propagates and thins while the stress remains nearly constant. We also provide a video of the tensile process, which directly shows the morphological evolution during stretching. This behavior can be understood on the basis of the double-network (DN) design principle. In our system, the first network has a relatively high crosslinking density and is therefore stiff and brittle, whereas the second network contains low crosslinker content and high monomer content, resulting in a loosely crosslinked and highly entangled network with improved toughness. Accordingly, in Stage I, both networks deform cooperatively. In Stage II, damage initiates in the brittle first network, leading to local crack formation and slight stress softening; at this stage, the first network acts as a sacrificial network for energy dissipation. In Stage III, the second network remains continuous and bears the load, while the entangled chains gradually slide, align, and extend along the tensile direction. This process gives rise to stable necking and progressive neck propagation at nearly constant stress, which is reflected as a plateau in the stress-strain curve. Such behavior is consistent with yielding or necking-dominated deformation reported in entanglement-rich hydrogel systems. Repeated tests on samples exhibiting the plateau show good reproducibility. Taken together, these results demonstrate that the plateau originates from the intrinsic deformation mechanism of the double network hydrogel, namely, damage initiation in the brittle first network followed by sustained load-bearing and necking propagation in the highly entangled second network, rather than from grip slippage or another experimental artifact.

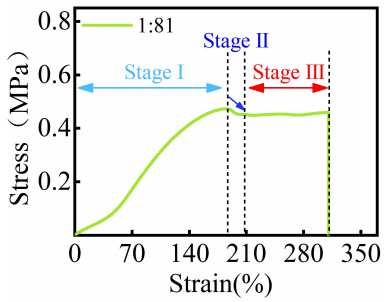

Figure S6. The tensile stress-strain curve of the hydrogel. For the first network, the AMPS, initiator and crosslinker are 0.01 M, 0.0006 M, and 0.0004 M, respectively. For the second network, the AM, SBVI, the initiator and the crosslinker are 0.1 M, 0.014 M, 0.0006 M, and 0.00061 M, respectively. The feed molar ratio of first and second network is from 1:81.

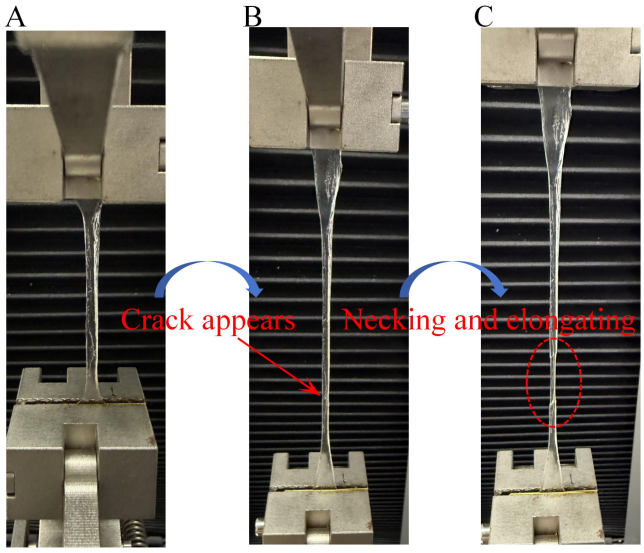

Figure S7. Morphological changes of the gel during stretching process. (A) initial stretching, (B) crack initiation, (C) gradual necking and elongation.

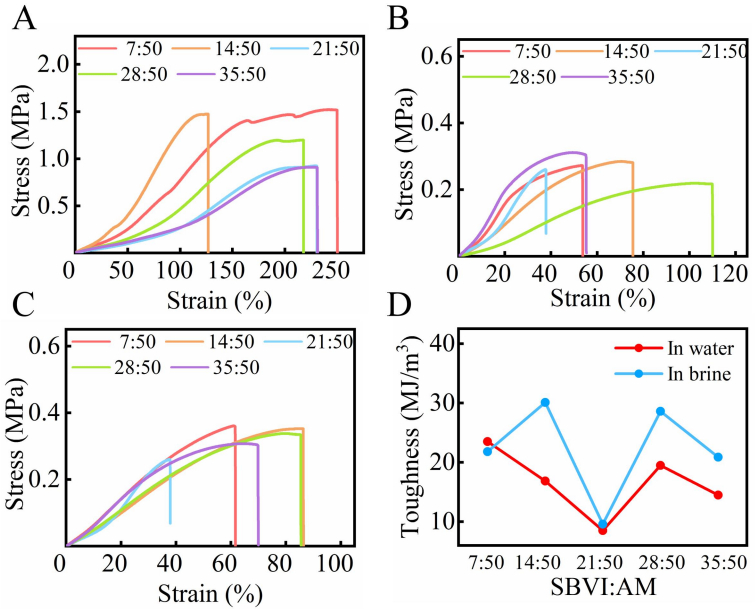

Figure S8. Systematic optimization of the monomer ratio for hydrogels. For the first network, the AMPS, initiator and crosslinker are 0.01 M, 0.0006 M, and 0.0004 M, respectively. The feed molar ratio of first and second network is 1:40. For the second network, the initiator and crosslinker are 0.0006 M, and 0.00031 M respectively. The monomer content is 0.07 M.(A) The stress-strain of the as-prepared hydrogels with different ratios. (B) The stress-strain of the water-swollen hydrogels with different ratios. (C) The stress-strain of the brine-swollen hydrogels with different ratios. (D) The toughness of water-swollen hydrogels and bine-swollen hydrogels with different ratios

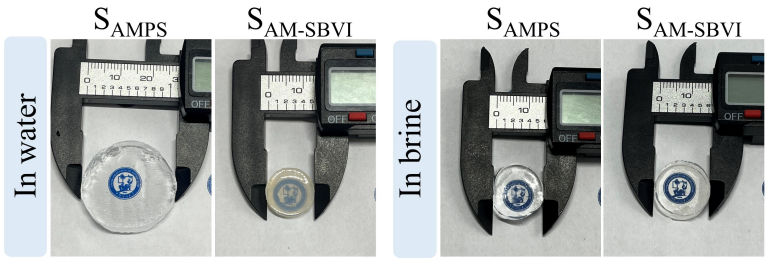

Figure S9. The morphological changes of S_{AMPS} and $S_{AM\text{-}SBVI}$ after swelling in water and brine (100 g/L NaCl).

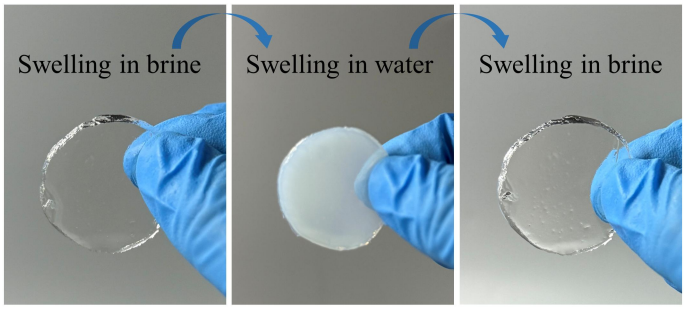

Figure S10. The morphological changes of $D_{AMPS/AM\text{-}SBVI}$ after swelling in water and brine (100 g/L NaCl).

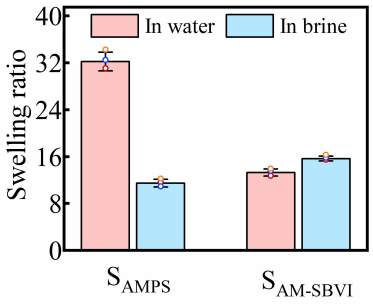

Figure S11. The swelling ratio comparison of S_{AMPS} and $S_{AM\text{-}SBVI}$. Mean ± SD, n = 3 independent samples.

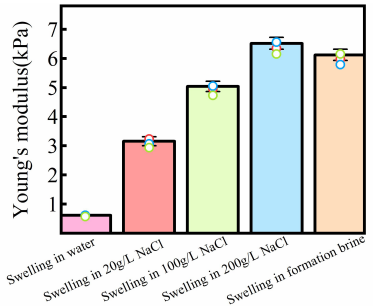

Figure S12. The Young's modulus of hydrogels swollen in different solutions. The Young's modulus of the hydrogels prepared swollen in varying conditions are calculated from the slope of the linear region (strain range: 10-20%) of the stress-strain curve. . Mean ± SD, n = 3 independent samples.

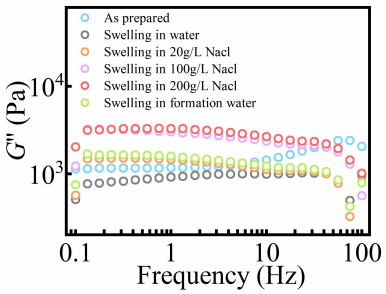

Figure S13. The loss modulus (*G*") of as-prepared and fully swollen hydrogels with 1% strain.

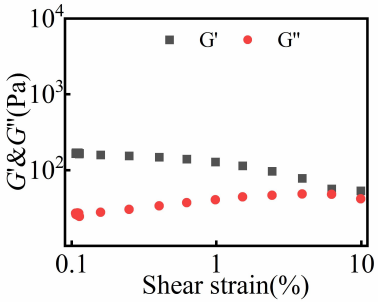

Figure S14. Strain sweep measurement of hydrogel swollen in 20 g/L NaCl.

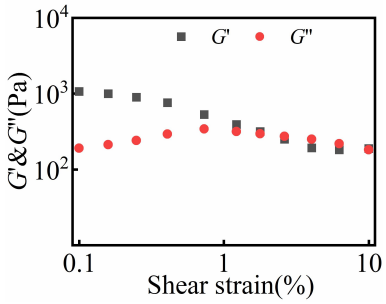

Figure S15. Strain sweep measurement of hydrogel swollen in 100 g/L NaCl.

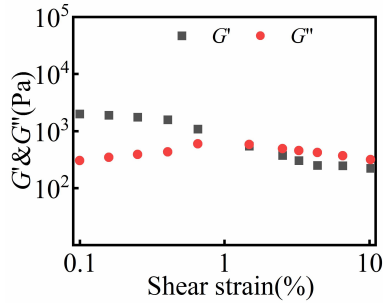

Figure S16. Strain sweep measurement of hydrogel swollen in 200 g/L NaCl.

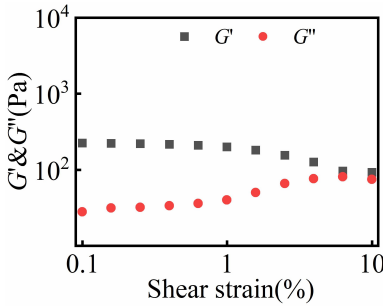

Figure S17. Strain sweep measurement of hydrogel swollen in formation brine.

Figure S18. Pictures demonstrating the contact angle of hydrogels after swelling in distilled water.

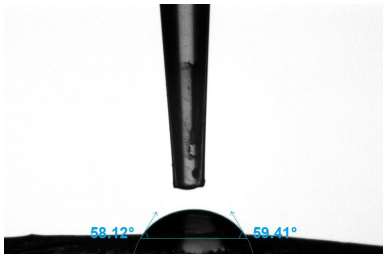

Figure S19. Pictures demonstrating the contact angle of hydrogels after swelling in brine.

Ion-dipole interactions

To further examine whether AM can interact with salt ions under brine conditions, FTIR analyses are performed on $D_{AMPS/SBVI}$ and $D_{AMPS/AM-SBVI}$ hydrogels. The C=O stretching band shifts from 1652 to 1646 cm^{-1} after swelling in brine, indicating that the local environment of the carbonyl group changes in saline solution, as shown in Figure S20. This spectral shift is consistent with altered carbonyl interactions, but does not by itself demonstrate a dominant binding mechanism.

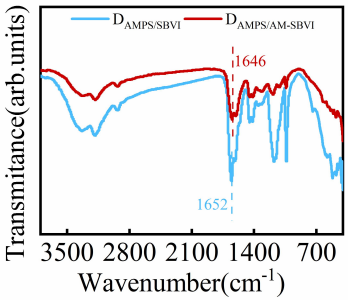

Figure S20. The FTIR of $D_{AMPS/SBVI}$ and $D_{AMPS/AM-SBVI}$ swelling in 100 g/L NaCl. $D_{AMPS/SBVI}$: The first network is AMPS and the second network is SBVI. $D_{AMPS/AM-SBVI}$: The first network is AMPS and the second network is AM and SBVI.

To further probe this possibility, we apply density functional theory (DFT) calculations for the interaction between Na^+ and the carbonyl oxygen of AM. The optimized geometry and electrostatic potential distribution show that Na^+ can interact with the carbonyl oxygen through electrostatic attraction, as illustrated in Figure S21. The binding energy is calculated as $E_{binding\ energy} = E_{(AM\text{-}Na^+)} - E_{(AM)} - E_{(Na^+)}$. The binding energy of the O-Na^+ complex is

-0.02345 eV, indicating that the interaction is energetically favorable but weak. Therefore, the DFT result supports the existence of an AM-Na^+ cation-dipole interaction, but does not support interpreting it as the dominant driving force for the macroscopic salt-enhanced mechanics or swelling. Instead, this weak interaction may act as an auxiliary factor that facilitates local chain relaxation and structural homogenization under saline conditions.

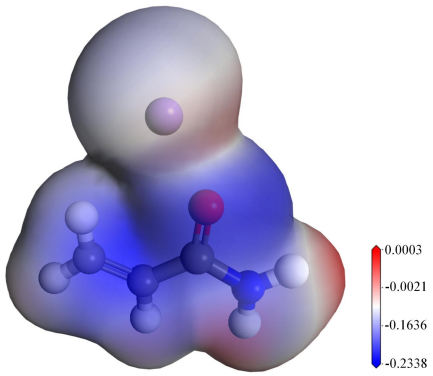

Figure S21. The electrostatic potential distribution of AM and Na^+.

Hydrogen bonding

The noncovalent interactions encompass a wide variety[11], including hydrogen bonding, electrostatic interactions, hydrophobic associations, π-π stacking, coordination complex formation, and so on. Among these, hydrogen bonding has relatively strong bond energy and has been widely employed by researchers through various engineering strategies to enhance the mechanical performance of hydrogels. In high AM content systems, hydrogen bonding is the most probable noncovalent inter- and intramolecular interaction. The strengths of hydrogen bonds vary widely, ranging from weak van der Waals interactions to hydrogen bonds with moderate strength and partial covalent properties. Since the development of the cellulose dissolution method by Zhang et al. in 2004[12], urea is generally considered and used as an efficient hydrogen bond breaker between polymer chains. To verify whether hydrogen bonding triggers changes in the network mechanical properties, we employ urea (8 wt%) to disrupt hydrogen bonding in hydrogels. The experimental procedures involve subjecting hydrogels to the following treatments: (#1) swelling in water, (#2) swelling in brine, (#3) swelling in urea followed by swelling in brine, and (#4) simultaneous swelling in both urea and brine. Rheological properties are then measured for each treatment group. After swelling

in water (#1), the hydrogel exhibits the lowest storage modulus (G') and loss modulus (G''), which are lower than those in brine-swollen hydrogels (#2), as shown in Figure S22 and Figure S23. The above rheological results further confirm the salt-enhanced mechanical behavior of our hydrogels. For the hydrogels swollen in brine (#2) and those swollen simultaneously in urea and brine (#4), the G' and G'' values are similar, indicating that disruption of hydrogen bonding does not eliminate the salt-enhanced mechanical response. Moreover, the hydrogel, pretreated with urea and subsequently swollen in brine (#3) exhibits the highest G' and G'' among all groups, suggesting that the break of hydrogen-bond constraints can facilitate later structural rearrangement in brine. These results indicate that hydrogen bonding is not the dominant origin of the mechanical enhancement observed after salt swelling.

3) Other interactions

Beyond hydrogen bonding and cation-dipole interaction, other AM-related weak interactions may exist after salt exposure. In the present system, these are more reasonably understood as nonspecific amide-amide dipole-dipole association, weak van der Waals contacts, salt-modulated local aggregation, and physical entanglement-assisted structural relaxation within the AM-containing second network, rather than as strong, well-defined directional bonds. Such effects may influence local morphology, chain packing, and baseline viscoelasticity of the hydrogel. However, based on the currently available evidence, we do not consider these AM-related interactions to be the dominant origin of the anomalous salt-enhanced co-improvement in swelling and mechanical strength.

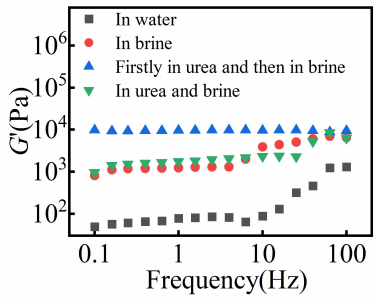

Figure S22. The storage modulus (G') of hydrogels with different treatments.

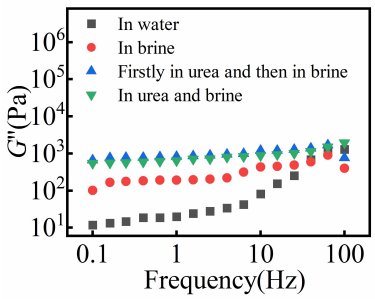

Figure S23. The loss modulus (G'') of hydrogels with different treatments.

The AM molar ratios in the second network is high. High AM content contributes to the overall network mechanics by increasing chain entanglement, improving chain flexibility, and providing a more deformable secondary network for energy dissipation. This point is supported by comparative rheological measurements, as shown in Figure S24 and Figure S25. The $D_{AMPS/SBVI}$ hydrogel exhibits lower storage modulus (G')and loss modulus (G'') than $D_{AMPS/AM-SBVI}$ after swelling in brine. However, the main focus of our work is not simply why the AM-containing hydrogel is mechanically stronger in an absolute sense, but rather why the same hydrogel becomes stronger after swelling in brine than in water. In other words, our key question concerns the differential enhancement (Δ) induced by salt exposure.

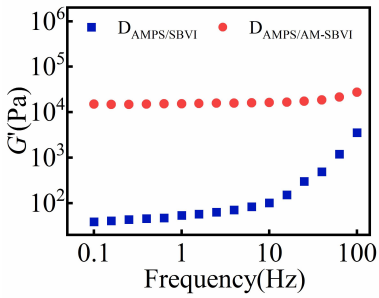

Figure S24. The storage modulus (G') of $D_{AMPS/SBVI}$ and $D_{AMPS/AM-SBVI}$ after swelling in brine. $D_{AMPS/SBVI}$: The first network is AMPS and the second network is SBVI. $D_{AMPS/AM-SBVI}$: The first network is AMPS and the second network is AM and SBVI.

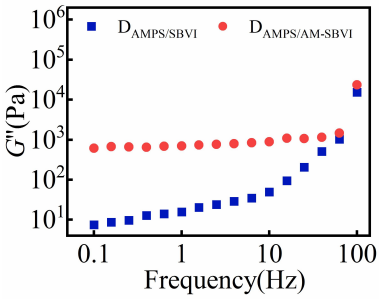

Figure S25. The loss modulus (G'') of $D_{AMPS/SBVI}$ and $D_{AMPS/AM-SBVI}$ after swelling in brine. $D_{AMPS/SBVI}$: The first network is AMPS and the second network is SBVI. $D_{AMPS/AM-SBVI}$: The first network is AMPS and the second network is AM and SBVI.

References

1. Xiao, S., *et al.* Salt-Responsive Bilayer Hydrogels with Pseudo-Double-Network Structure Actuated by Polyelectrolyte and Antipolyelectrolyte Effects. *ACS Applied Materials & Interfaces* **9**, 20843-20851 https://doi.org/10.1021/acsami.7b04417 (2017).
2. Huang, K.-T., Ishihara, K. & Huang, C.-J. Polyelectrolyte and Antipolyelectrolyte Effects for Dual Salt-Responsive Interpenetrating Network Hydrogels. *Biomacromolecules* **20**, 3524-3534 https://doi.org/10.1021/acs.biomac.9b00796 (2019).
3. Zheng, S. Y., *et al.* A Molecularly Engineered Zwitterionic Hydrogel with Strengthened Anti-Polyelectrolyte Effect: from High-Rate Solar Desalination to Efficient Electricity Generation. *Advanced Functional Materials* **33**, 2303272 https://doi.org/https://doi.org/10.1002/adfm.202303272 (2023).
4. Ren, J., *et al.* Super-Tough, Non-Swelling Zwitterionic Hydrogel Sensor Based on the Hofmeister Effect for Potential Motion Monitoring of Marine Animals. *Advanced Materials* **36**, 2412162 https://doi.org/https://doi.org/10.1002/adma.202412162 (2024).
5. Ni, H., *et al.* Zwitterionic Microgel-Reinforced Hydrogels with Low Hysteresis and High Toughness for Electrochemical Applications. *ACS Applied Materials & Interfaces* **18**, 4283-4292 https://doi.org/10.1021/acsami.5c20932 (2026).
6. Li, X., *et al.* High-Strength and Nonfouling Zwitterionic Triple-Network Hydrogel in Saline Environments. *Advanced Materials* **33**, 2102479 https://doi.org/https://doi.org/10.1002/adma.202102479 (2021).
7. Gao, H., *et al.* Euryhaline Hydrogel with Constant Swelling and Salinity-Enhanced Mechanical Strength in a Wide Salinity Range. *Advanced Functional Materials* **31**, 2007664 https://doi.org/https://doi.org/10.1002/adfm.202007664 (2021).
8. Liu, X., Ji, X., Zhu, R., Gu, J. & Liang, J. A Microphase-Separated Design toward an All-Round Ionic Hydrogel with Discriminable and Anti-Disturbance Multisensory Functions. *Advanced Materials* **36**, 2309508 https://doi.org/https://doi.org/10.1002/adma.202309508 (2024).
9. Zeng, J., Chen, H., Dong, L. & Guo, X. Anti-Polyelectrolyte Effect of Zwitterionic Hydrogel Electrolytes Enabling High-Voltage Zinc-Ion Hybrid Capacitors. *Advanced Functional Materials* **34**, 2314651 https://doi.org/https://doi.org/10.1002/adfm.202314651 (2024).
10. Aleid, S., *et al.* Salting-in Effect of Zwitterionic Polymer Hydrogel Facilitates Atmospheric Water Harvesting. *ACS Materials Letters* **4**, 511-520 https://doi.org/10.1021/acsmaterialslett.1c00723 (2022).
11. Zhao, Y. H., *et al.* Universal law of hierarchical dynamics in gels arising from confluence of local physically dynamic bonds. *Nature Communications* **16**, 3247 https://doi.org/10.1038/s41467-025-58571-2 (2025).

12. Cai, J.*, et al.* Novel Fibers Prepared from Cellulose in NaOH/Urea Aqueous Solution. *Macromolecular Rapid Communications* **25**, 1558-1562 https://doi.org/https://doi.org/10.1002/marc.200400172 (2004).